Meteoritics & Planetary Science 38, Nr 4, 485–499 (2003)
Abstract available online at http://meteoritics.org

KREEPy lunar meteorite Dhofar 287A: A new lunar mare basalt

Mahesh ANAND,[1*] Lawrence A. TAYLOR,[1] Kula C. MISRA[1], Svetlana I. DEMIDOVA,[1, 2] and Mikhail A. NAZAROV[1, 2]

[1]Planetary Geosciences Institute, University of Tennessee, Knoxville, Tennessee 37996, USA
[2]Vernadsky Institute of Geochemistry and Analytical Chemistry, Moscow 11975, Russia
[*]Corresponding author. E-mail: anandm@utk.edu

(Received 25 April 2002; revision accepted 11 October 2002)

Abstract–Dhofar 287 (Dho 287) is a new lunar meteorite, found in Oman on January 14, 2001. The main portion of this meteorite (Dho 287A) consists of a mare basalt, while a smaller portion of breccia (Dho 287B) is attached on the side. Dho 287A is only the fourth crystalline mare basalt meteorite found on Earth to date and is the subject of the present study. The basalt consists mainly of phenocrysts of olivine and pyroxene set in a finer-grained matrix, which is composed of elongated pyroxene and plagioclase crystals radiating from a common nucleii. The majority of olivine and pyroxene grains are zoned, from core to rim, in terms of Fe and Mg. Accessory minerals include ilmenite, chromite, ulvöspinel, troilite, and FeNi metal. Chromite is invariably mantled by ulvöspinel. This rock is unusually rich in late-stage mesostasis, composed largely of fayalite, Si-K-Ba-rich glass, fluorapatite, and whitlockite. In texture and mineralogy, Dho 287A is a low-Ti mare basalt, with similarities to Apollo 12 (A-12) and Apollo 15 (A-15) basalts. However, all plagioclase is now present as maskelynite, and its composition is atypical for known low-Ti mare basalts. The Fe to Mn ratios of olivine and pyroxene, the presence of FeNi metal, and the bulk-rock oxygen isotopic ratios, along with several other petrological features, are evidence for the lunar origin for this meteorite.

Whole-rock composition further confirms the similarity of Dho 287A with A-12 and A-15 samples but requires possible KREEP assimilation to account for its rare-earth-element (REE) contents. Cooling-rate estimates, based on Fo zonation in olivine, yield values of 0.2–0.8°C/hr for the lava, typical for the center of a 10–20 m thick flow. The recalculated major-element concentrations, after removing 10–15% modal olivine, are comparable to typical A-15 mare basalts. Crystallization modeling of the recalculated Dho 287A bulk-composition yields a reasonable fit between predicted and observed mineral abundances and compositions.

INTRODUCTION

Most studies of lunar rocks and soils have been conducted on samples collected by the U.S. Apollo and Soviet Luna missions, but these represent samples from <10% of the lunar surface. However, recent discoveries of meteorites blasted off the moon have provided new impetus to lunar research. Such meteorites are being discovered regularly in the hot deserts of Oman and Northern Africa and in the icefields of Antarctica. In the past 2 decades, more than 30 lunar meteorites have been discovered from these locales. Many of these meteorites are probably from areas on the moon, far removed from those sampled by the Luna or Apollo missions. More importantly, only 4 of them are meteorites of lunar mare basalts. These are invaluable samples because they provide further insight into lunar petrogenetic history.

Dho 287 is a new lunar meteorite that was found in the Dhofar region of Oman on January 14, 2001. It is a dark-gray stone weighing 154 g that does not have any fusion crust. The rock is strongly shocked, with impact-melt veins. Terrestrial weathering features are mainly iron staining and oxidation, along with invading carbonate veins. This meteorite actually consists of two adjacent lithologies: mare basalt (Dho 287A) that comprises about 95% of the rock and regolith breccia (Dho 287B) that forms about 5% by volume of the sample. Taylor et al. (2001b) have given an initial classification and preliminary mineralogical and textural description of this meteorite. Although Dhofar 025 was found but 400 m from Dho 287, these two meteorites are definitely not paired. A detailed mineralogical and petrological investigation has been performed on Dho 287A, and the petrological features of this meteorite have been compared with basalt samples returned by lunar missions, as well as with other lunar mare basalt meteorites (Y-793169, A-881757, and NWA 032).

Our studies have been performed on 3 polished thin sections with a total area of 3.8 cm^2. In addition, collaborative work among different labs has provided an adequate geochemical dataset from which we are able to infer the petrogenetic history of Dho 287A.

ANALYTICAL METHODS

Polished thin sections of Dho 287A were examined to study the textural and mineralogical characteristics. Mineral modes were determined using Feature Scan software with an Oxford Instrument Energy Dispersive Spectral (EDS) unit. This is part of an automated CAMECA SX-50 electron microprobe (EMP) at the University of Tennessee. Mineral compositions were determined with the EMP using an accelerating potential of 15 KeV, 20 nA beam current, 1 μm beam size, and standard ZAF (PAP) correction procedures. The counting times were 20 s for the majority of elements; the counting times for V and Zr were 60 and 90 s, respectively. For maskelynite analyses, a beam current of 10 nA and a beam size of 7 μm were used to avoid Na volatilization. Similarly, a current of 10 nA and beam size of 10 μm were used for glass analysis.

About 1 g of the sample was crushed and powdered in an agate mortar for major- and trace-element determinations. XRF and ICP-MS analyses were performed for Si, Ti, Al, Cr, Fe, Mn, Mg, and Ca. Na and K were determined by atomic absorption. Trace-elements (REEs, Sc, Co, Cr, etc.) were analyzed by instrumental neutron activation analysis (INAA). These analyses were conducted at the Vernadsky Institute, Moscow, Russia. Bulk-rock oxygen isotope determination was conducted at the University of Chicago following the procedure of Clayton and Mayeda (1963, 1983).

PETROGRAPHY AND MINERAL CHEMISTRY

The lunar meteorite Dho 287A is a coarse-grained basalt consisting mainly of phenocrysts of olivine (>1–2 mm) and pyroxene (up to 0.5 mm) set in a finer-grained matrix, which is composed of elongated pyroxene and plagioclase crystals, radiating from common nucleii (Fig. 1a). The distribution of silicate minerals in Dho 287A is highly variable. In some areas of the rock, phenocrysts of olivine and pyroxene predominate over plagioclase feldspar (Fig. 1b), while other areas in the rock are predominantly composed of plagioclase and pyroxene (Figs. 1c and 1d). Another conspicuous feature of olivine and pyroxene grains is the presence of numerous cracks and fractures that are probably due to shock. The same shock event seems to have converted all plagioclase into maskelynite (Figs. 1b–1f). Partial masking of maskelynite grains by a thin veneer of pyroxene is noticed in many cases (Fig. 1f), but its significance is unknown.

Accessory minerals in Dho 287A include ilmenite, chromite rimmed by ulvöspinel, troilite, and FeNi metal, and they seem to occur in clusters in the rock (Fig. 1d). Similar to olivine and pyroxene, the chromite grains also contain shock-induced fractures. However, in the majority of cases, these cracks conspicuously terminate at the chromite-ulvöspinel boundary. Another feature of the rock is the cocrystallization of ilmenite and plagioclase (Figs. 1c–1d).

The modal mineralogy of Dho 287A, as determined by the X-ray digital-imaging procedure, described by Taylor et al. (1996), is given in Table 1. Data for other mare basalt meteorites and some A-12 and A-15 mare basalts are also listed in Table 1. Note that Dho 287A has the highest modal olivine and the lowest modal plagioclase compared to the other mare basalts listed. The effect of this is readily apparent in terms of bulk-rock major-element chemistry, which is discussed in the next section. The most distinctive petrographic feature of Dho 287A is the unusual abundance (>3%) of late-stage mesostasis, which is composed mainly of fayalite, Si-K-Ba-rich glass, fluorapatite, and whitlockite. The mesostasis areas, common to many lunar basalts, show the typical "swiss cheese" pattern that is easily identifiable in reflected light.

In terms of texture and mineralogy, Dho 287A is a low-Ti mare basalt, with similarities to A-12 and A-15 basalts, but more akin to the olivine normative basalts (ONB) of A-15 samples. However, the plagioclase in Dho 287A has been completely converted to maskelynite and, as discussed below, its composition is atypical of such basalts. In the following sub-sections, detailed characteristics of individual minerals are described.

Olivine

Olivine in Dho 287A occurs as phenocrysts (>1–2 mm), most with chemical zonation. They are present as elongated to equant grains with orange iron-oxide staining, as seen in plane-polarized light. This staining is somewhat more pronounced in the cores of olivines, which can be attributed either to terrestrial alteration of Mg-rich cores or to shock effect (Ostertag et al. 1984). Some of the olivine grains show asymmetrical zoning with extreme iron enrichment (up to Fo_{40}) within 20–50 μm of the rims. This observation can be explained by the fact that only free sides of early-formed olivines were in contact with the melt, which was enriched in Fe. Nevertheless, the majority of the olivine grains show symmetrical normal zoning.

EMP data for a number of olivine grains (~100), from two polished thin sections, were collected to obtain the range in Fo contents, as shown in Fig 2a. The representative compositions of the mineral phases present in Dho 287A are listed in Table 2. The bimodal distribution in Fo contents reflects the occurrence of Mg-rich olivines ($Fo_{40–70}$) as phenocrysts, and fayalitic olivines ($Fo_{0–15}$) in the mesostasis areas of the rock. The petrographic similarity of Dho 287A to A-12 and A-15 basalts is also evident in terms of mineral

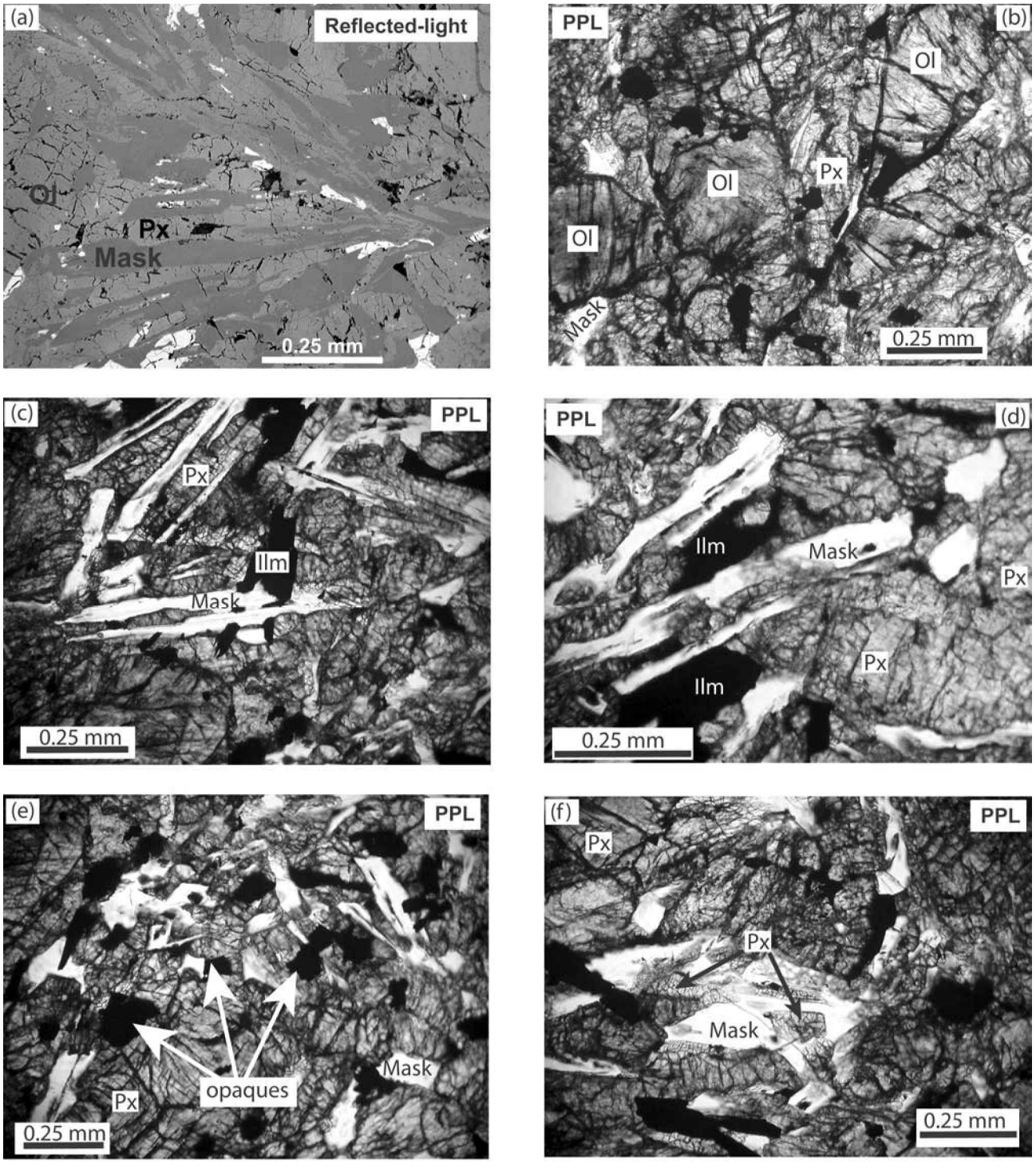

Fig. 1. Photomicrographs illustrating textures and mineralogy of Dho 287A. The typical radial texture of the rock is defined by laths of maskelynite (Mask) and pyroxene (Px) originating from a common nucleii (a). Heterogeneous distribution of constituent minerals is seen in different areas of the thin section. Euhedral to subhedral olivine (Ol) phenocrysts generally occur in clusters together with pyroxene (b). Laths of maskelynite show co-crystallization texture with ilmenite (c and d). Some areas contain high concentration of opaque minerals (spinel and ilmenite) (e). Partial masking of maskelynite grains by a thin veneer of pyroxene is noticed in many cases (f).

Table 1. Modal abundances (vol%) in mare basalt meteorites and similar basalts from Apollo 12 and 15.[a]

	Mare basalt meteorites					Apollo 12 and 15 basalts		
	Dho 287A	NWA 032	Y-793169	A-881757	EET 87521 (clast A)	12016,25	12054	15556;136
Olivine phenocrysts	20.6	11.3	0	0	15	12	10.8	0.1
Chromite phenocrysts	0.4	0.3	0	<5	–	0	1.9	0.4
Pigeonite	29.3	–	–	–	–	–	–	–
Augite	15.7	–	–	–	–	–	–	–
Fe-pyroxene	2.4	–	–	–	–	–	–	–
Undifferentiated pyroxene	47.4	50.7	56	59	44	52.1	62.1	57
Feldspar/maskelynite	25.9	29.4	42	30	39	29.1	27.9	38
Ilmenite	2.3	4.4	1	6	2	4.8	5.2	2.1
Ulvöspinel	0.8	tr	1	<5	0	0	0.5	0.6
Troilite	0.1	0.7	0	<5	0	0	0.3	0.1
FeNi metal	tr	tr	0	<5	0	0	0.1	tr
Opaque minerals (total)	3.6	5.4	2	<11	2	4.8	8	3.2
Silica	0.2	0	0	0	0	0	0.1	0.8
Phosphate	0.6	–	–	–	–	–	–	–
Fayalite	0.2	–	–	–	–	–	–	–
Melt glass	1.4	3.2	0	0	0	0	0	0
Volcanic glass/mesostasis	>3	0	0	0	0	0.6	1.9	1

[a]Data sources: Dho 287A, Anand et al. (2002); NWA 032, Fagan et al. (2001); Y-793169, Takeda et al. (1993); A-881757, Yanai and Kojima (1991); EET 87251 clast A, Warren and Kallemeyn (1989); 12016 and 12054, Neal et al. (1994); 15556, Rhodes and Hubbard (1973).

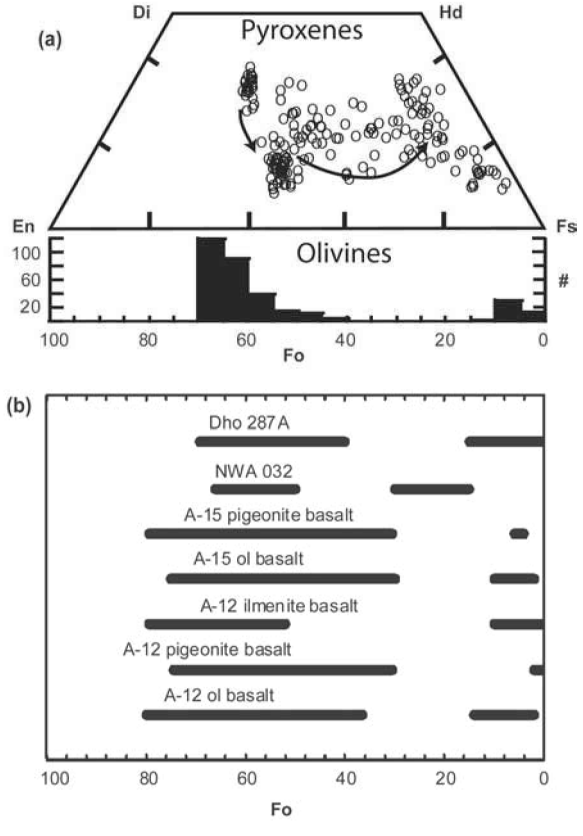

Fig. 2. Compositions of pyroxenes and olivines in Dho 287A: a) pyroxene compositions range from augite-pigeonite to pyroxferroite. The histogram shows the bimodal distribution in Fo contents of olivine grains; b) comparison of olivine Fo contents in Dho 287A with those of other low-Ti mare basalts. The data source for NWA 032 is Fagan et al. (2001), and for the Apollo samples is BVSP (1981).

compositions (Fig. 2b). Because of its mineralogical similarity to Dho 287A, data for mare basalt NWA 032 are also plotted. Since Dho 287A is a low-Ti olivine-normative basalt, it is mainly compared and contrasted with A-12 and A-15 olivine-basalt samples in subsequent sections.

The variation in the Fo contents of several olivine grains was also investigated by collecting probe data along two orthogonal profiles in each grain. A backscattered electron image (BSE) of one such grain is shown in Fig. 3a. The variations in Fo content along two orthogonal profiles in this olivine grain are plotted in Fig 3b. Note the sharp decrease in Fo content in the outer zones of the crystal. Minimum cooling-rate estimations (Taylor et al. 1977), based on variation in Fo content in several olivine grains along orthogonal profiles, yield values of 0.2–0.8°C/hr for these olivines, corresponding to the center of a 10–20 thick lava flow. Such cooling rates are typical of mare basalts.

Pyroxene

Pyroxene is the most abundant mineral in Dho 287A and occurs as both phenocrysts and groundmass crystals. The phenocrysts are generally elongated (normally >0.5 mm) and show similar petrographic features to that of olivine, albeit with less iron staining. A thin veneer of pyroxene with extensive fractures occurs within some maskelynite (Fig. 1f), probably formed during the shock event, perhaps the same event responsible for the launch of this meteorite from the moon.

Pyroxene compositions show extreme variation in terms of Ca-Mg-Fe contents (Fig. 2a), following a typical mare basalt fractionation trend. Similar to olivines, pyroxenes in Dho 287A also show normal zoning with extreme Fe-enrichments in their outer portions. The late-stage ferro-pyroxene mainly occurs in the vicinity of the mesostasis areas

Table 2. Representative electron microprobe analyses (wt%) of constituent minerals in Dho 287A.[a]

Phases	Pyroxene	Fe-Px[b]	Olivine	Fayalite	Plagioclase	K-Ba-glass	Si-glass	Apatite	Whitlockite	Ilmenite	Chromite	Ulvöspinel
SiO_2	49.5	45.1	36.9	29.6	48.2	76.9	97.5	0.93	5.83	na	na	na
TiO_2	1.17	0.95	na	na	na	0.34	0.34	0.02	0.12	51.0	4.69	27.9
Al_2O_3	1.25	1.05	na	na	31.6	11.2	1.72	0.15	1.46	0.08	12.3	2.98
Cr_2O_3	0.26	<0.03	0.24	na	na	na	na	na	na	0.05	45.2	10.5
MgO	10.8	1.29	32.3	1.19	0.19	<0.03	<0.03	0.18	2.06	0.10	2.16	0.55
CaO	11.8	5.77	0.42	0.91	16.6	0.28	0.54	53.5	41.0	0.30	0.07	0.03
MnO	0.34	0.55	0.36	0.67	na	0.03	0.04	<0.03	0.15	0.36	0.30	0.33
FeO	24.5	44.6	29.7	66.3	0.60	0.47	0.35	2.20	4.98	46.4	34.1	56.6
Na_2O	0.06	<0.03	na	na	1.87	0.53	0.21	0.04	0.46	na	na	na
K_2O	na	na	na	na	0.11	6.57	<0.03	0.05	0.22	na	na	na
NiO	na	na	0.03	na	na	na	na	na	na	na	na	na
SO_3	na	na	na	na	na	<0.03	<0.03	0.33	0.37	na	na	na
BaO	na	na	na	na	na	3.33	<0.03	na	na	na	na	na
P_2O_5	na	na	na	na	na	0.03	<0.03	40.8	41.1	na	na	na
ZrO_2	na	na	na	na	na	na	na	na	na	0.39	na	0.15
V_2O_3	na	na	na	na	na	na	na	na	na	na	0.71	0.43
Cl	na	na	na	na	na	na	na	0.17	0.07	na	na	na
F	na	na	na	na	na	na	na	2.47	0.05	na	na	na
Total	99.8	99.3	99.9	98.7	99.1	99.7	100.7	100.9	97.8[c]	98.6	99.6	99.5
Oxygen basis	6	6	4	4	8	24	24	25	25	3	4	4
Si	1.943	1.941	0.998	1.004	2.231	10.200	11.718	0.156	0.948	–	–	–
Ti	0.034	0.031	–	–	–	0.034	0.031	0.002	0.014	0.985	0.122	0.772
Al	0.058	0.053	–	–	1.726	1.754	0.243	0.029	0.279	0.002	0.504	0.129
Cr	0.008	–	0.005	–	–	–	–	–	–	0.001	1.239	0.305
Mg	0.633	0.083	1.304	0.060	0.013	–	–	0.045	0.500	0.004	0.112	0.030
Ca	0.498	0.266	0.012	0.033	0.825	0.039	0.070	9.637	7.134	0.008	0.003	0.001
Mn	0.011	0.020	0.008	0.019	–	0.004	0.004	–	0.021	0.008	0.009	0.010
Fe	0.803	1.608	0.672	1.879	0.023	0.052	0.035	0.309	0.677	0.996	0.988	1.739
Na	0.005	–	–	–	0.168	0.137	0.048	0.014	0.146	–	–	–
K	–	–	–	–	0.006	1.112	0.004	0.011	0.045	–	–	–
Ni	–	–	0.001	–	–	–	–	–	–	–	–	–
S	–	–	–	–	–	–	–	0.052	0.056	–	–	–
Ba	–	–	–	–	–	0.173	–	–	–	–	–	–
P	–	–	–	–	–	0.004	–	5.812	5.647	–	–	–
Zr	–	–	–	–	–	–	–	–	–	0.005	–	0.003
V	–	–	–	–	–	–	–	–	–	–	0.020	0.013
Total	3.99	4.00	3.00	3.00	4.99	13.5	12.2	16.1	15.5	2.01	3.00	3.00
Mg#	44.1	4.91	66.0	3.09	–	–	–	–	–	–	–	–
Fe#	55.9	95.1	34.0	96.9	–	–	–	–	–	–	–	–
An #	–	–	–	–	82.6	–	–	–	–	–	–	–
Cr #	–	–	–	–	–	–	–	–	–	–	66.4	25.3

[a]na = not analyzed.
[b]Fe-Px = Pyroxferroite.
[c]REE detectable in EDS but not measured.

where its composition approaches pyroxferroite. However, it is very important to note that these Fe-rich compositions occur only at the outer margins of pyroxene grains that are immediately in contact with the mesostasis (i.e., late-stage fractionate).

Feldspar

Plagioclase in Dho 287A has been completely converted into maskelynite, probably by processes associated with the ejection of this meteorite from the moon. This is the first reported occurrence of total conversion of plagioclase to maskelynite in a lunar basalt. The maskelynite occurs in irregular shapes (Fig. 1), with the majority present as elongated grains forming a radial pattern along with pyroxenes and originating from common nucleii (Fig. 1a). Some areas in the thin sections appear anomalous, particularly associated with feathery pyroxene, and there is evidence for minor melting. Based on the plagioclase that has only undergone long-range disordering to transform to diaplactic glass (instead of melting), the shock pressure was estimated to be about 30 GPa (Stöffler et al. 1991).

Maskelynite compositions show the typical fractionation trend seen in most mare basalt plagioclases (Fig. 4a). Compared to plagioclases in A-12 and A-15 basalts, maskelynite in this rock is unusually rich in Ab content. The

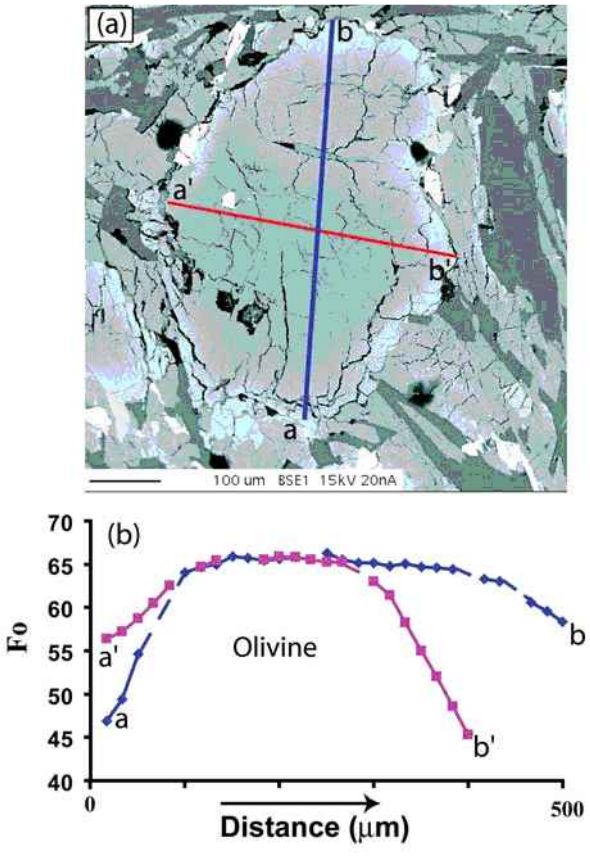

Fig. 3. a) Backscattered electron (BSE) image of an olivine grain in Dho 287A. The two orthogonal lines indicate the traverses along which EMP data were collected; b) plot of variation in Fo contents along the two orthogonal profiles a-b and a'-b'. Note extreme Fe-enrichment in the outer 20–50 μm of the rim of the grain.

An contents of Dho 287A maskelynite vary from 85 to 73 compared to An values of 87 or higher for A-12 and A-15 basalts.

Opaques

Opaque minerals are abundant (i.e., ~3–4%) throughout Dho 287A. Ilmenite is the most common opaque mineral, occurring as lath-shaped grains (Figs. 1b and 1e) and in some cases, shows lamellar structure, indicative of shock features (Taylor et al. 1971). Compositionally, ilmenites are essentially $FeTiO_3$, with no significant geikielite ($MgTiO_3$) (<0.5 wt% MgO) or pyrophanite ($MnTiO_3$) (<0.4 wt% MnO) components.

Spinels are the second most abundant of the opaque minerals and occur in the form of aluminous chromite rimmed by ulvöspinel (Fig. 5). In reflected-light (oil immersion), chromite appears bluish, while ulvöspinel appears tan in color, making the distinction between the two relatively straightforward. Generally, ilmenite and spinel occur in clusters, although they are only rarely in direct contact with each other (Fig. 5). Evidence for typical sub-

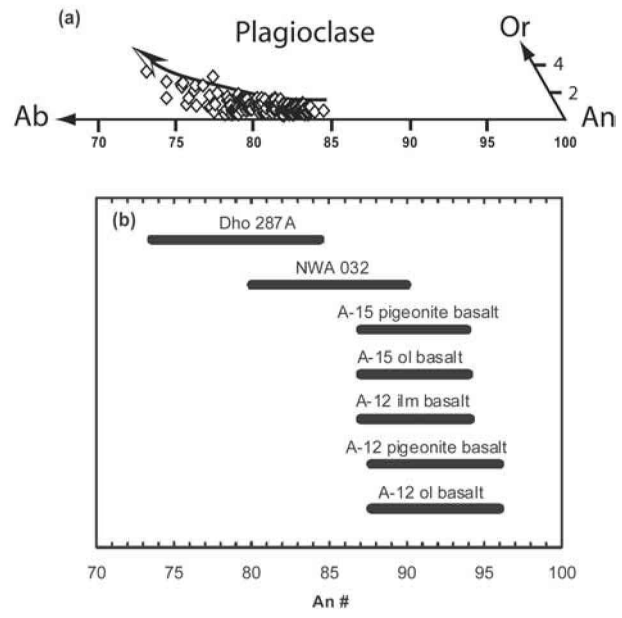

Fig. 4. a) Maskelynite analyses plotted in the Or-Ab-An ternary diagram. The maskelynite compositions follow the typical mare basalt trend. Maskelynite in Dho 287A is relatively An poor, and its composition is atypical of known lunar mare basalts; b) comparison of plagioclase An contents in Dho 287A with that of other low-Ti mare basalts. The data source for NWA 032 is Fagan et al. (2001), and for the Apollo samples is BVSP (1981).

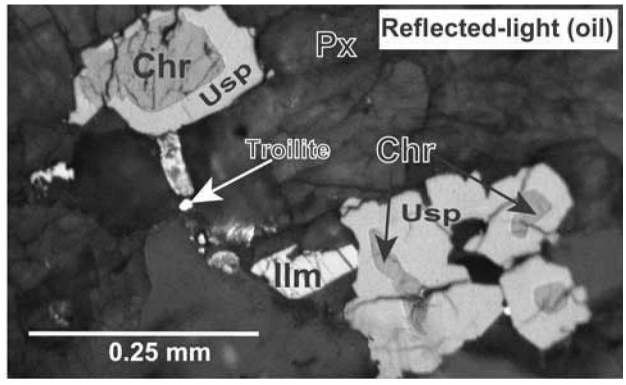

Fig. 5. Reflected-light image (oil immersion) of Dho 287A showing chromite (Chr) grains rimmed by ulvöspinel (Usp). Note that the fractures in chromite do not generally propagate across chromite-ulvöspinel boundaries. An ilmenite grain is also seen in the middle of the photomicrograph touching an ulvöspinel grain.

solidus reduction of ulvöspinel to ilmenite + Fe metal, although rare, is present, as seen in most mare basalts. The boundary between chromite and ulvöspinel appears to be sharp; the intermediate compositions are most likely due to "edge-effects." Dho 287A spinel data follow a fractionation trend similar to those seen for spinels in A-12 and A-15 mare basalts (Figs. 6a and 6b) (El Goresy 1976; Taylor et al. 1971).

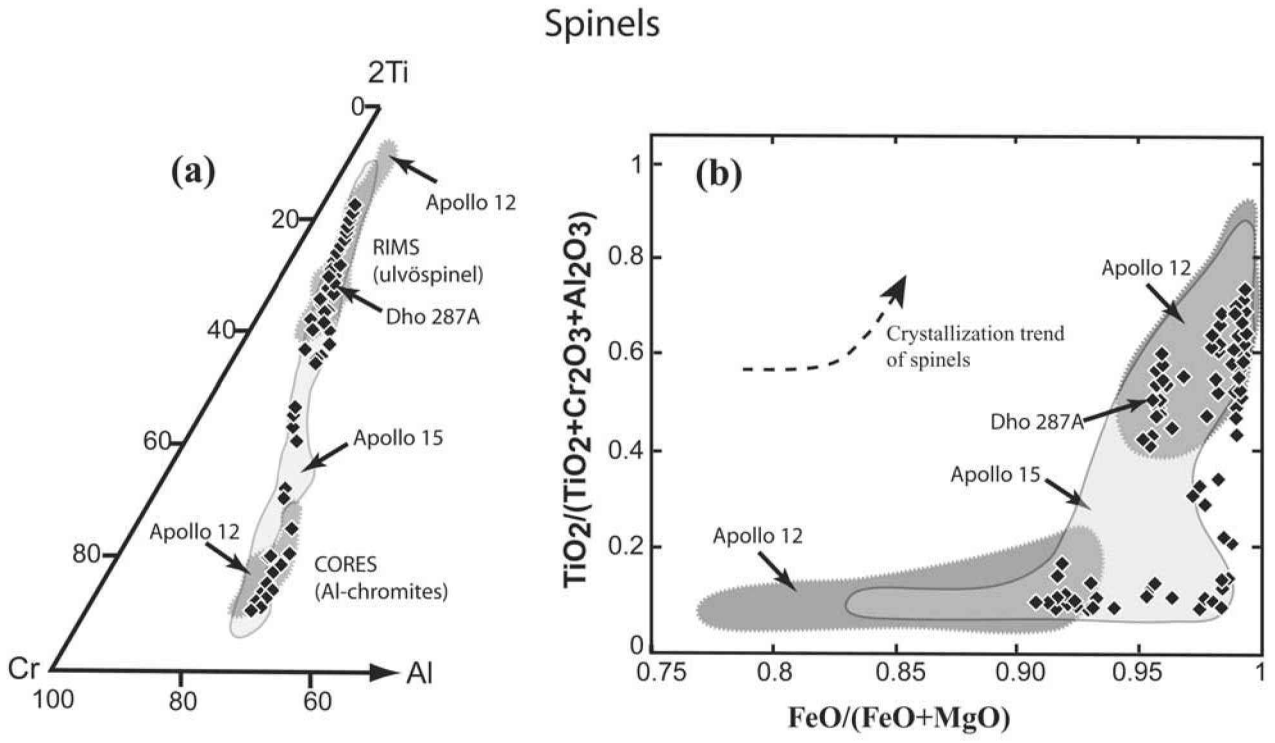

Fig. 6. a) Spinel analyses plotted on a typical ternary plot of 2Ti-Cr-Al (in mol%). The spinel compositions follow the lunar trend defined by the Apollo 12 and 15 samples; b) a plot of FeO/(FeO+MgO) versus $TiO_2/(TiO_2+Cr_2O_3+Al_2O_3)$ (in wt%) for Dho 287A spinels also shows a crystallization trend similar to that defined by A-12 and A-15 spinels.

FeNi metal and troilite (FeS) also occur, albeit sparsely distributed. The Ni and Co contents in FeNi metals show a large range (<0.03–39.6 wt% Ni; <0.03–2.1 wt% Co). The highest Ni values are in the metal grains enclosed by olivine, but both olivine and pyroxene seem to contain inclusions of high-Ni metal. A metal grain enclosed by pyroxene contains two "patches" of high-Ni (22 to 28 wt%) in a matrix of lower Ni (5–7 wt%) metal, a possible taenite-kamacite association. The Co contents range from 0.5 to 1.6 wt%.

Mesostasis

A feature found in many lunar basalts is the late-stage fractionation product represented by the mesostasis. One of the most striking petrographic features of Dho 287A is the disproportionately large abundance (>3%) of late-stage mesostasis throughout the sample. A typical mesostasis area shows a "swiss cheese" texture (Figs. 7a and 7b), consisting of fayalite (cheese) and glass (holes in cheese). The presence of 2 different sized, chemically different glass blebs is clearly seen in the mesostasis areas. These areas are typically 300 × 300 μm in size, composed mainly of fayalite, both Si-rich and K-Ba-rich glasses, ilmenite, apatite, and whitlockite (Fig. 7), and with an overall KREEPy chemistry. Pyroxene grains surrounding mesostasis areas show extreme iron enrichment, all the way to pyroxferroite. Fig. 7b shows a typical mesostasis area with a large bleb of K-Ba-rich glass. In the upper half of the picture, two stages of intergrowth between fayalite and K-rich glass are present. Needles of apatite, whitlokite, and laths of ilmenite occur randomly throughout the mesostasis areas.

Various mineral phases (Table 2) present in the mesostasis areas can be considered to be the product of silicate liquid immiscibility (SLI), as described by numerous authors (Hess et al. 1978; Neal and Taylor 1989, 1991; Rutherford et al. 1974). SLI only occurs after 95 to 98% fractionation of a magma, as it splits it into a K fraction (granitic) and REEP fraction (ferrobasaltic). The ferrobasaltic portion can subsequently undergo further fractional crystallization, forming fayalite, ilmenite, apatite, whitlockite, and SiO_2 glass (e.g., Neal and Taylor 1989). The granitic melt portion has high viscosity, and upon rapid cooling, it quenches to glass, forming silica-rich pods. In Dho 287A mesostasis areas, the K-Ba-Si-rich glasses represent the K fraction, and the ilmenite, fayalite, and phosphate assemblage correspond to the REEP fraction (Neal and Taylor 1989). An interesting feature of the mesostasis in Dho 287A is the presence of two different types of glass compositions: a) K-Ba-rich glass; and b) a relatively K-poor but silica-rich glass, mainly associated with REEP melt fraction. A few glass compositions are almost pure SiO_2. This probably resulted from extreme fractionation of the melt from which this rock formed. It is not the presence of, but the unusually high abundance of KREEPy mesostasis

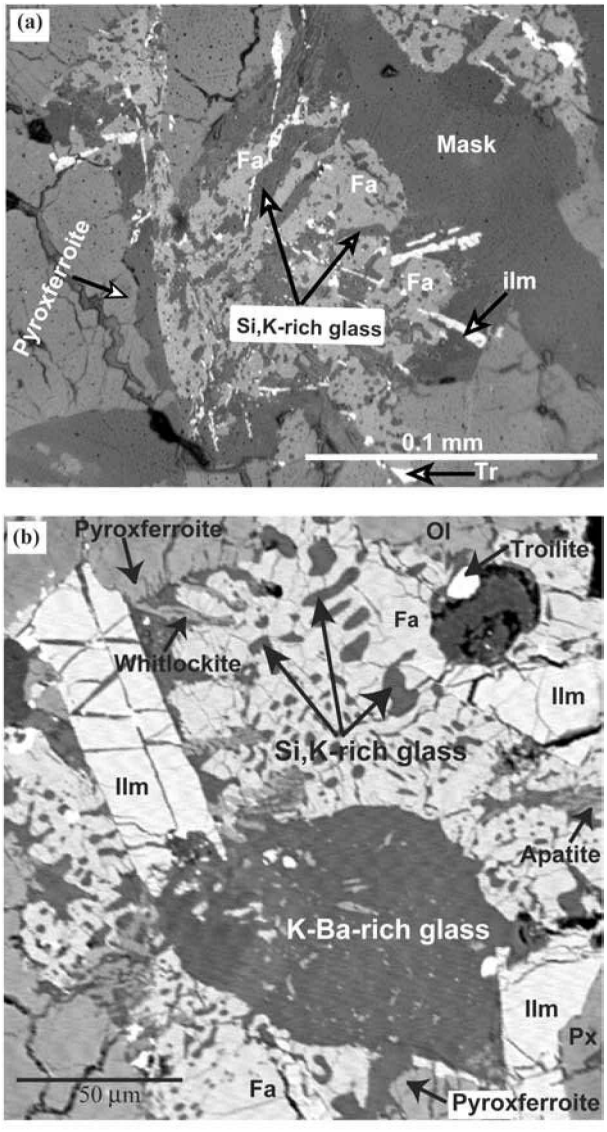

Fig. 7. a) Reflected light view of a mesostasis area illustrating the typical "swiss cheese" texture. The light gray areas are composed of fayalite (Fa) and K-Si-rich glass. Fe-pyroxene surrounds the mesostasis area. Brighter spots indicate troilite grains; b) BSE image of another mesostasis area showing intergrowth of fayalite and Si-K-rich glass in the upper and lower half of the picture. Note two generations of intergrowth, evident in terms of sizes of exsolved glass phase. Pyroxene and olivine (Ol) grains surrounding the area show extreme iron enrichment, which appears in a lighter shade of gray compared to relatively Mg-rich cores that appear darker in color.

in this rock that may be evidence for KREEP assimilation (Ringwood and Kesson 1976).

LUNAR ORIGIN

Constituent minerals in rocks from different planetary bodies are well known to have different Fe to Mn ratios (Drake et al. 1989). Rocks from the earth, moon, Mars, HED parent body, and chondrites (i.e., asteroid belt) show distinct trends in Fe to Mn ratios in their mafic phases (Papike 1998). This feature has been successfully used to identify source regions for meteorites. In the case of Dho 287A, the Fe to Mn ratios in olivines and pyroxenes follow the typical lunar trend (Figs. 8a and 8b), evidence for the lunar origin of this meteorite.

Bulk-rock $\delta^{18}O$ and $\delta^{17}O$ values for Dho 287A are +6.20‰ and +3.24‰, respectively, and these are among the highest measured oxygen isotopic values for a lunar sample (Fig. 9). Nevertheless, Dho 287A oxygen isotopic data plot on the terrestrial fractionation line, along with other lunar samples, and when considered in conjunction with the Fe to Mn ratios of olivine and pyroxene grains, provide further evidence for the lunar origin of this meteorite and exclude the possibility of it being any unusual HED meteorite. These unusually high $\delta^{18}O$ and $\delta^{17}O$ values for Dho 287A are, however, most likely due to the effects of terrestrial alteration in the hot-desert environment, as has been suggested previously in the case of meteorites from Algeria (Stelzner et al. 1999).

Additional evidence of a lunar origin for this meteorite is the presence of FeNi metal. Virtually all mare basalts contain primary and secondary FeNi metal, a direct effect of the low fO_2 prevalent in lunar magmatic systems. The abundant KREEPy mesostasis as a late-stage fractionate is yet another evidence, as is the overall geochemistry (see the petrogenesis section). Major evidence of lunar genesis is found in the radiogenic isotope data. Sm-Nd isotopic determination on 4 bulk-rock (leachates and residues) and 2 pyroxene-rich samples yielded a good linear array, corresponding to an age of 3.46 ± 0.03 Ga (Shih et al. 2002), comparable in age with that of A-12 and A-15 samples. This age probably represents the original crystallization age of the basalt. However, the ε_{Nd} ratio calculated for Dho 287A at 3.46 Ga is −0.63 ± 0.32, which is very different from other high-Ti or low-Ti mare basalts, possibly indicating some KREEP assimilation.

PETROGENESIS

Whole-Rock Geochemistry

The selected whole-rock, major-, trace- and rare-earth-element data for Dho 287A and other similar mare basalts are presented in Table 3. Compared to other low-Ti lunar mare basalts, Dho 287A has higher MgO and FeO and lower CaO and Al_2O_3 contents. This is most probably due to the higher-modal abundance of olivine in the rock. In addition, this rock has relatively higher abundances of Na_2O, K_2O, and other incompatible elements. This can be the result partly of the effects of terrestrial alteration in a desert environment (mostly for Na) and the result partly of KREEP assimilation. Therefore, Dho 287A appears to be an atypical mare basalt,

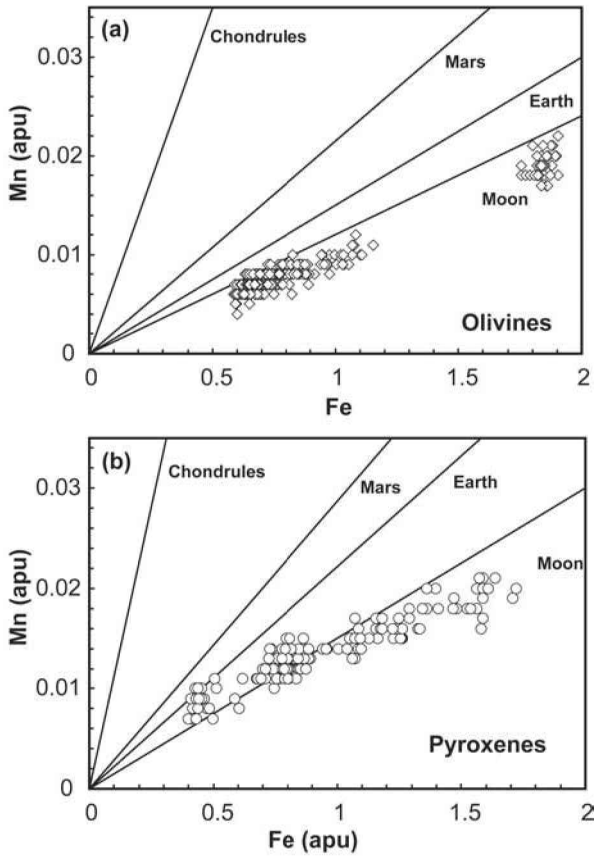

Fig. 8. Fe/Mn ratios (in mol%) in olivines (a) and pyroxenes (b) from Dho 287A follow lunar trend, confirming a lunar origin for this meteorite. The Fe/Mn trends for the other parent bodies are from Papike (1998).

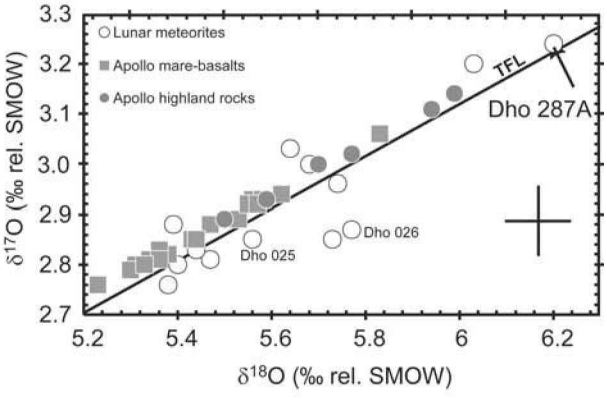

Fig. 9. Oxygen isotopic compositions of Dho 287A plot along the terrestrial fractionation line (TFL), also defined by other lunar meteorites and Apollo rocks. The data source for the lunar meteorites is from Clayton and Mayeda (1996). The data on the Apollo samples are from Wiechert et al. (2001), and the Dho 025 and Dho 026 values are from Taylor et al. (2001a). The plus sign on the plot indicates the analytical uncertainty in $\delta^{17}O$ and $\delta^{18}O$ measurements for the lunar meteorites.

which seems to have a distinct petrogenetic history compared to any other known low-Ti mare basalt.

Lunar mare basalts are classified according to their TiO_2 contents into three separate groups: high (TiO_2 >6 wt%), low (TiO_2 1–6 wt%), and very low (TiO_2 <1 wt%) titanium basalts (Neal and Taylor 1992). Based on this classification scheme, Dho 287A can be classified as a low-Ti mare basalt (Fig. 10a), similar to A-12 and A-15 mare basalts. In Fig. 10, data for mare basalts returned from both Apollo and Luna missions (compiled from various sources) have also been shown for comparison. Similarly, other bivariate diagrams have been used to compare and contrast the geochemical features of Dho 287A with basalts from the Apollo and Luna missions. Fig. 10a, shows that the Mg# of Dho 287A is toward the higher end of the range defined by lunar basalts, suggesting its primitive nature. However, this rock is depleted in Al_2O_3 (Fig. 10b) and CaO content and slightly enriched in FeO content compared to A-12 and A-15 low-Ti mare basalts (Fig. 10b), which can be interpreted as an indication of a possible cumulate portion for this rock. Therefore, the high bulk-rock Mg# is probably due to the presence of cumulate olivine. These observations are consistent with the petrographic and mineralogic data that confirm the high modal olivine content in the rock, as well as the presence of Fe-enriched mineral phases and the low-plagioclase content in the rock.

The bulk-rock trace-, and REE compositions indicate the LREE-enriched and HREE-depleted nature of Dho 287A. On a plot of La versus Yb (Fig. 11a), it is evident that Dho 287A is enriched in La and relatively poorer in Yb, giving a very high $(La/Yb)_n$ value (2.7) to the rock compared to the range seen in other mare basalts (0.7–1.8). Sm-enrichment and the negative Eu anomaly, characteristic of all mare basalts, are highlighted on a plot of Sm versus Sm/Eu (Fig. 11b).

On a chondrite-normalized REE plot, Dho 287A shows a relatively steep REE pattern, a distinctive feature of this rock (Fig. 12). REE data for other low-Ti mare basalt meteorites and A-12 and A-15 basalts are also plotted for comparison. Dho 287A and NWA 032 seem to have similar LREE patterns but differ significantly in terms of their HREE contents. Lunar mare basalt meteorites (except NWA 032 and EET 87521 clast) and A-12 and A-15 mare basalts show positive slopes in their LREE patterns compared to the negative slope shown by Dho 287A. Overall, the most conspicuous feature of the Dho 287A REE pattern is the steep LREE/HREE pattern compared to other mare basalts. Although the A-15 basalt shows a steep HREE pattern similar to Dho 287A, it has a positive LREE slope.

The LREE-enriched nature of Dho 287A may partially be ascribed to the effects of terrestrial weathering (Crozaz and Wadhwa 2001). However, the HREEs are among the least mobile elements in a basaltic rock, and the steep negative pattern seen in Dho 287A may well be a source characteristic rather than an artifact of terrestrial alteration. An important

Table 3. Major- and trace-element composition of mare basalt meteorites and similar basalts from Apollo 12 and 15.[a]

	Mare basalt meteorites					Apollo 12 and 15 basalts			
	Dho 287A	NWA 032	Y-793169	A-881757	EET 87521 (clast A)	12016, 9	12054, 62	15119, 19	15556, 177
wt%		1	2	2	3	4	4	5	5
SiO_2	43.2	44.7	46.0	47.1	48.4	42.8	45.9	44.9	45.7
TiO_2	2.76	3.08	2.19	2.45	1.13	4.02	4.63	2.57	2.62
Al_2O_3	8.35	8.74	11.1	10.0	12.5	7.23	10.5	8.96	9.48
Cr_2O_3	0.65	0.40	0.24	0.29	0.21	0.57	0.33	0.59	0.84
FeO	22.1	23.0	21.2	22.5	19.2	22.6	19.5	22.2	21.7
MnO	0.29	0.33	0.32	0.34	0.24	0.30	0.29	0.28	0.28
MgO	13.2	8.45	5.75	6.30	6.30	12.7	6.76	9.38	8.15
CaO	8.74	10.9	12.0	11.8	11.7	8.42	11.9	10.0	10.6
Na_2O	0.53	0.37	0.27	0.25	0.41	0.22	0.31	0.26	0.26
K_2O	0.19	0.11	0.06	0.04	0.07	0.06	0.07	0.05	0.05
P_2O_5	0.21	–	–	–	–	0.08	0.06	0.07	0.07
LOI	0.10	–	–	–	–	–	–	–	–
Total	100.3	99.7	99.2	101.0	100.0	99.0	100.2	99.2	99.6
Mg #	51.5	39.6	32.6	33.3	37.3	49.9	38.2	43.0	40.1
µg/g									
Sc	35.2	56	93.7	99.4	44	–	–	44	46
Co	42.3	42	29.8	27.9	46	54	31	50	50
Ni	20	50	53	52	29	25	–	59	63
Sr	530	142	78	115	104	126	162	112	101
Zr	60	175	59	45	140	117	128	95	94
Ba	200	242	34	27	88	59	64	44	44
La	12.9	11.2	4.72	3.69	8.3	–	–	5.36	5
Ce	30.3	29.7	14.8	10.9	20.9	16.2	18.8	15.9	15.8
Nd	20.4	21	11.9	8.31	13	–	–	15	13
Sm	6.31	6.61	4.3	2.88	3.86	5.5	6	3.82	3.65
Eu	1.18	1.1	1.31	1.1	0.98	1.06	1.27	0.94	0.96
Tb	1.22	1.56	1.02	0.76	0.8	1.42	1.85	0.83	0.87
Yb	3.35	5.79	4.59	3.26	3.19	5	5.8	2.36	2.27
Lu	0.51	0.8	0.66	0.52	0.48	0.67	0.78	0.32	0.31
Hf	2.64	5	3.01	2.2	2.88	6.3	4.8	2.89	2.89
Ta	0.71	0.62	0.31	0.22	0.37	–	–	0.41	0.39
Th	0.9	1.9	0.68	0.42	0.95	–	–	0.49	0.46

[a]Data sources: 1) Fagan et al. (2001); 2) major elements from Warren and Kallemeyn (1993) and minor elements from Koeberl et al. (1993); 3) Warren and Kallemeyn (1989); 4) Rhodes et al. (1977); 5) Ryder and Schuraytz (2001).

note, however, is that in Fig. 12, the REE pattern for KREEP is similar in slope to that of Dho 287A, and hence, assimilation of KREEP-rich material by the Dho 287A parental magma may have occurred. This could explain the unusually high abundance of mesostasis and incompatible elements in Dho 287A. Mixing calculations for REEs between a typical A-15 mare basalt (15119, 19) and ~8% KREEP yield similar chondrite-normalized REE patterns to those of Dho 287A, thereby supporting the fact that KREEP-rich material was assimilated in the Dho 287A parental magma (Table 4; Fig. 12).

Although the plagioclase content of Dho 287A is lower than NWA 032, it still has a higher absolute abundance of Eu, though with a smaller Eu-anomaly compared to the latter. This discrepancy may be explained by KREEP assimilation, which raises the absolute Eu abundance in the rock. However, at the same time, it is expected that KREEP assimilation in Dho 287A lava should increase the Eu anomaly in the resulting rock, but this is not so in the present case. The smaller Eu* in Dho 287A compared to NWA 032 seems to be the result of anomalously low HREE contents of Dho 287A (especially Gd). Assimilation of KREEPy material could also account for the disproportionately high abundance of the late-stage mesostasis, rich in incompatible elements, within Dho 287A.

There are various ways by which KREEP can be assimilated in a mare basalt magma. One possible scenario is that KREEP was assimilated in the magma, at higher levels, perhaps just before eruption of the lava. This assimilation would be followed by crystal fractionation to maintain the heat budget of the system. This is consistent with the presence of cumulate olivines in Dho 287A compared to typical low-Ti mare basalts. The other possibility involves the addition of KREEP to the source region of the mare basalt, Dho 287A, followed by the melt generation event. This process is plausibly related to mantle overturn or injection due to a large

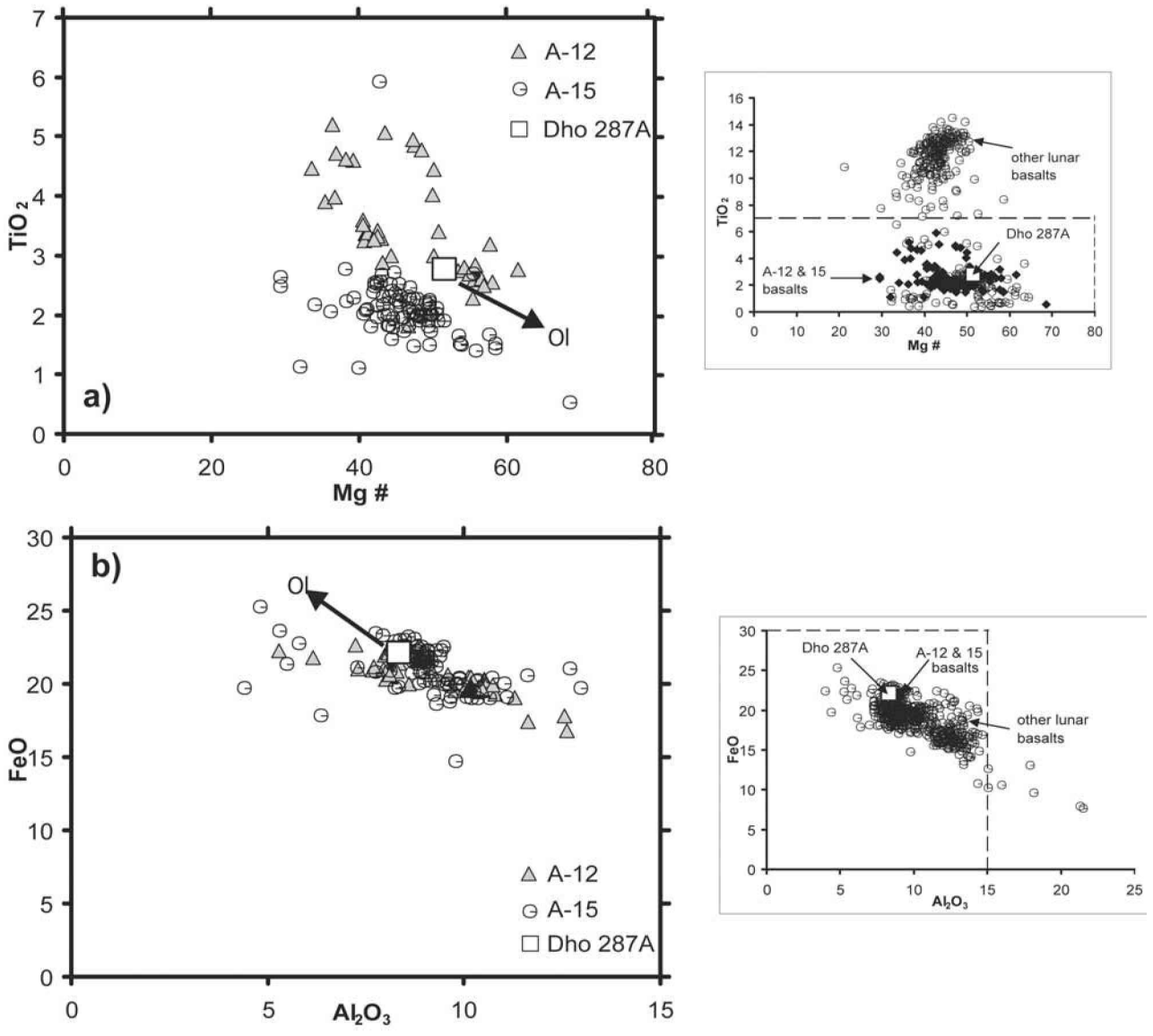

Fig. 10. Variation diagrams for selected whole-rock major-element data for Dho 287A. The data for the A-12 and A-15 mare basalts are also plotted for comparison. The figures on the right show the complete data set available for mare basalts from the Apollo and Luna missions. The figures on the left are enlargements of the rectangular boxes outlined by dashed lines on the respective figures on the right: a) the Mg# versus TiO_2 plot confirms Dho 287A to be a low-Ti mare basalt, according to the classification of Neal and Taylor (1992). Dho 287A is similar, but relatively high in Mg#, to the majority of Apollo 12 and 15 mare basalt samples; b) the Al_2O_3 versus FeO plot indicates that Dho 287A is also enriched in FeO content but has low Al_2O_3 content compared to other low-Ti mare basalts. The arrows indicate the olivine control line.

impact event. However, in the present case, the former process is favored over the latter, as it adequately characterizes the mineralogy and geochemistry of Dho 287A.

Crystallization Modeling

The modal mineralogy of Dho 287A, as well as its geochemical characteristics, indicates appreciable olivine accumulation in the parental magma. The highest measured Fo content in Dho 287A olivine (Fo_{70}) is too low to be in equilibrium with a bulk-rock Mg# of 51.5. Using the TiO_2-calibrated Kd of 0.32 (Delano 1980), the calculated Fo content of olivine that is in equilibrium with a whole rock Mg# 51.5 is about 77. There is a difference of 6–7 Fo units between the calculated and observed Fo contents in the olivines of Dho 287A. To have a difference of 2–3 Fo units in basalts is common, but normally, not this much. This alone points to the possibility of cumulate olivine. In addition, the higher MgO and FeO versus lower Al_2O_3 and CaO of the bulk-rock is simply a function of cumulate olivine and is consistent with the unusually high modal proportion (21%) of olivine in the rock, which is not common in mare-basalts.

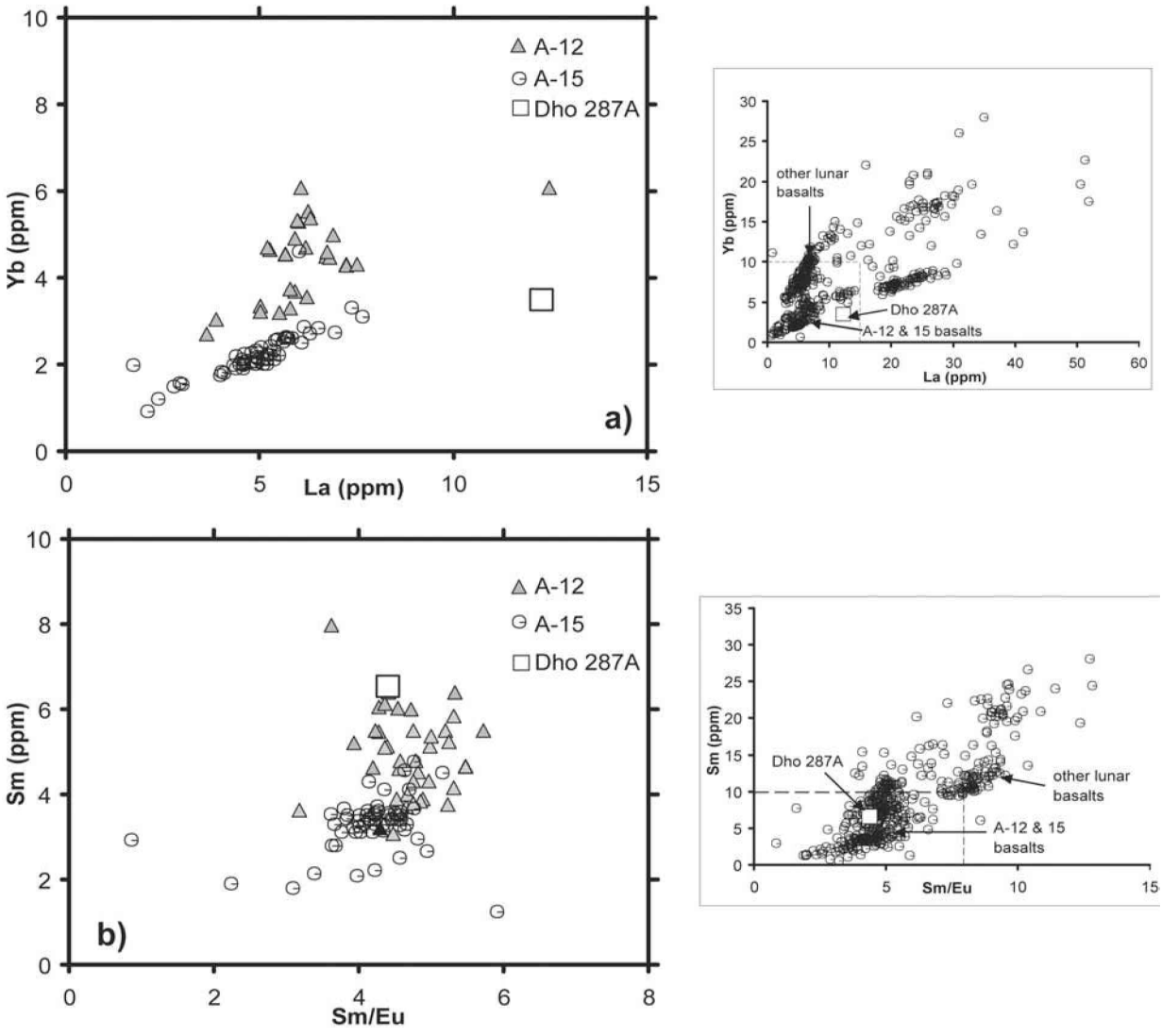

Fig. 11. Variation diagrams for selected whole-rock trace-element data for Dho 287A. The data for the A-12 and A-15 mare basalts are also plotted for comparison. The figures on the right show the complete data set available for mare basalts from the Apollo and Luna missions. The figures on the left are enlargements of the rectangular boxes outlined by dashed lines on the respective figures on the right: a) the La versus Yb plot highlights the LREE-enriched and HREE-depleted nature of Dho 287A; b) the Sm/Eu versus Sm plot indicates LREE enrichment in Sm and the presence of negative Eu anomaly, characteristic of all lunar mare basalts.

Therefore, the preceding discussion makes it evident that before we carry out crystallization modeling, we need to recalculate the original bulk-composition by removing the effects of olivine accumulation. Including the effects of KREEP assimilation in our crystallization modeling is difficult because the modeling mainly uses the major-element chemistry of the rock, which is not appreciably affected by KREEP assimilation. This assumption was crosschecked by comparing the results of crystallization models on a typical A-15 low-Ti mare basalt (such as 15119, 19) similar to Dho 287A that was not affected by any KREEP material.

The recalculated bulk-rock composition of Dho 287A, after 10–15% olivine removal (Table 4), has been modeled using the MELTS software of Ghiorso and Sack (1995). The results of both fractional and equilibrium crystallization modeling are presented in the form of bar diagrams in Fig. 13. The modeling was performed starting with a liquidus temperature of 1350°C and an oxygen fugacity equivalent to the Iron-Wustite (IW) buffer. Both equilibrium and fractional crystallization modeling provide a good match between the predicted and observed compositional ranges for the majority of mineral phases, but fractional crystallization provides a better fit to the observed mineral variations in the rock. This observation is consistent with the crystallization scenario expected for a lava flow. However, there are some discrepancies in the predicted range of plagioclase compositions; observed plagioclase compositions are relatively lower in An content than predicted. Nevertheless, crystallization modeling

Table 4. Recalculated Dho 287A bulk-composition after 12% olivine removal and mixing calculations between 15119, 19 and KREEP.

wt%	Dho 287A	After 15% ol removal	15119, 19 plus 8% KREEP
SiO_2	43.2	44.1	44.9
TiO_2	2.76	3.24	2.57
Al_2O_3	8.35	9.75	8.96
Cr_2O_3	0.65	0.70	0.59
FeO	22.1	21.3	22.2
MnO	0.29	0.29	0.28
MgO	13.2	9.35	9.38
CaO	8.74	10.2	10.0
Na_2O	0.53	0.62	0.26
K_2O	0.19	0.22	0.05
P_2O_5	0.21	0.25	0.07
LOI	0.10	–	–
Total	100.32	100.02	99.26
Mg #	51.5	43.8	42.9
µg/g			
Sc	35.2	35.2	–
Co	42.3	42.3	–
Ni	20	20	–
Sr	530	530	119
Zr	60	60	–
Ba	200	200	94.7
La	12.9	12.9	10.0
Ce	30.3	30.3	28.0
Nd	20.4	20.4	–
Sm	6.31	6.31	5.82
Eu	1.18	1.18	1.06
Tb	1.22	1.22	1.22
Yb	3.35	3.35	3.74
Lu	0.51	0.51	0.51
Hf	2.64	2.64	4.54
Ta	0.71	0.71	0.59
Th	0.9	0.9	1.29

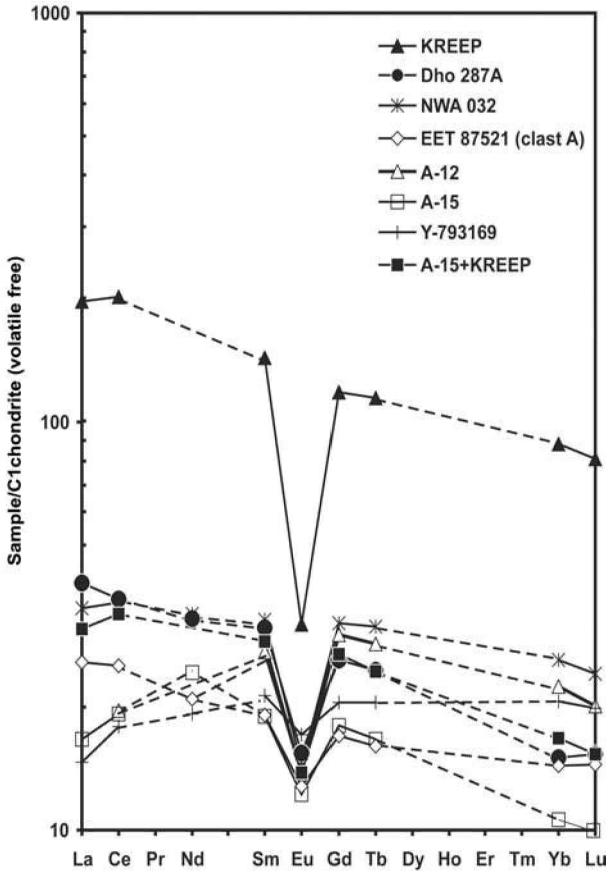

Fig. 12. Volatile-free, chondrite-normalized plot of REEs in Dho 287A. REE concentrations are normalized to those of volatile free CI-chondrites, i.e., 1.36C, where C is the "Mean C1 Chondrite" value for each element in Table 1 of Anders and Grevesse (1989). Three other mare basalt meteorites, one representative analysis each of Apollo 12 and 15 mare basalts, and KREEP are also plotted for comparison. The data source for the mare basalts is Fagan et al. (2000); KREEP data are from C. R. Neal (personal communication).

confirms that the mineralogy of Dho 287A is compatible with the scenario in which accumulation of olivine accompanied the crystallization of a Dho 287A parental liquid.

MELTS modeling of 15119, 19 bulk-composition predicts similar ranges in mineral compositions to that seen in Dho 287A. This result further suggests the possible affinity of Dho 287A to the A-15 low-Ti mare basalt suite, yet with some distinct characteristics that can be ascribed to the minor differences in source regions of these mare basalts.

SUMMARY

Dho 287A is a new lunar meteorite of a low-Ti mare basalt, which is unique in several respects compared to other lunar basalts. Based on the present study, the following aspects of Dho 287A are highlighted:

- Evidence for lunar origin: Fe to Mn ratios of olivine and pyroxene; presence of FeNi metal; bulk-rock oxygen isotopic ratios.
- Similar in texture and mineralogy to A-12 and A-15 low-Ti mare basalts; pyroxene compositions typical for low-Ti mare basalts, with progressive Fe-enrichment towards pyroxferroite.
- Distinctive features:
  - Unusually high abundance of mesostasis.
  - All plagioclase has been converted to maskelynite, first for mare basalts.
  - Negative initial ε_{Nd} isotopic composition.
- Whole-rock REE data
  - LREE-enrichment; high $(La/Yb)_n$.
  - REE content appears to be direct function of abundant KREEPy mesostasis.
  - REE contents modeled as mixture of ~8% KREEP and typical low-Ti mare basalt (e.g., 15119, 19).
- Overall petrological and mineralogical characteristics of Dho 287A: New variation of low-Ti mare basalts, similar to those from A-12 and A-15.

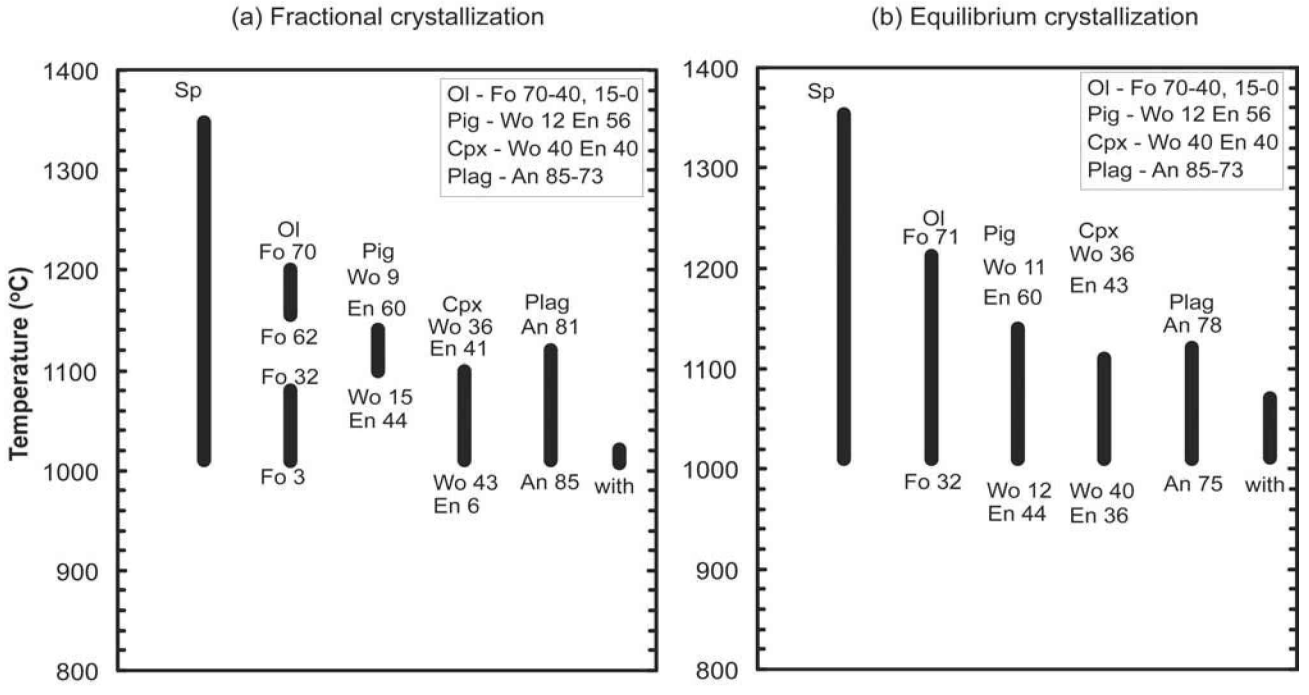

Fig. 13. Results of fractional (a) and equilibrium (b) crystallization modeling of the recalculated bulk rock composition of Dho 287A using the MELTS software of Ghiorso and Sack (1995). The inserts on each figure show the observed compositional ranges of Dho 287A silicates. Fractional crystallization modeling provides a better fit between observed and predicted mineral compositions. Equilibrium crystallization modeling failed to account for fayalitic olivines in Dho 287A and predicted a longer range in pigeonite composition.

Acknowledgments–We thank Allan Patchen for assistance with microprobe analyses and Dawn Taylor for assistance with graphics software packages. R. N. Clayton and T. K. Mayeda are thanked for providing oxygen isotope data. Critical and constructive reviews by Chip Shearer and Marc Norman helped to enhance the quality of the paper. This research has been supported through NASA grants NAG 5–10414 and NAG 5–11558 to L. A. Taylor and a RFBR grant 02–05–64981 to M. A. Nazarov.

Editorial Handling—Dr. Ross Taylor

REFERENCES

Anand M., Misra K. C., Taylor L. A., Cahill J. and Nazarov M. 2002. Apparently KREEPy lunar meteorite Dhofar 287A: The residual melt tapped from a fractionating magma chamber (abstract #1635). 33rd Lunar and Planetary Science Conference. CD-ROM.

Anders E. and Grevessen N. 1989. Abundances of the elements: Meteoritic and solar. *Geochimica et Cosmochimica Acta* 53:197–214.

Basaltic Volcanism Study Project. 1981. Lunar mare basalts. In *Basaltic volcanism on the terrestrial planets.* New York: Pergamon Press. pp. 236–281.

Clayton R. N. and Mayeda T. K. 1963. The use of bromine pentafluoride in the extraction of oxygen from oxides and silicates for isotopic analysis. *Geochimica et Cosmochimica Acta* 27:43–52.

Clayton R. N. and Mayeda T. K. 1983. Oxygen isotopes in eucrites, shergottites, nakhlites, and chassignites. *Earth and Planetary Science Letters* 62:1–6.

Clayton R. N. and Mayeda T. K. 1996. Oxygen isotope studies of achondrites. *Geochimica et Cosmochimica Acta* 60:1999–2017.

Crozaz G. and Wadhwa M. 2001. The terrestrial alteration of Saharan Shergottites Dar al Gani 476 and 489: A case study of weathering in a hot desert environment. *Geochimica et Cosmochimica Acta* 65:971–978.

Delano J. W. 1980. Chemistry and liquidus phase relations of Apollo 15 red glass: Implications for the deep lunar interior. Proceedings, 11th Lunar and Planetary Science Conference. pp. 251–288.

Drake M. J., Newsom H. E., and Capobianco C. J. 1989. V, Cr, and Mn in the earth, moon, EPB, and SPB and the origin of the moon: Experimental studies. *Geochimica et Cosmochimica Acta* 53: 2101–2111.

El Goresy A. 1976. Oxide minerals in lunar rocks. In *Oxide minerals,* edited by Rumble D. Mineralogical Society of America. pp. EG1–43.

Fagan T. J., Bunch T. E., Wittke J. H., Jarosewich E., Clayton R. N., Mayeda T., Eugster O., Lorenzetti S., Keil K., and Taylor G. J. 2000. Northwest Africa 032, a new lunar mare basalt. *Meteoritics & Planetary Science* 35:A51–A52.

Fagan T. J., Taylor G. J., Keil K., Bunch T. E., Wittke J. H., Korotev R. L., Jolliff B. L., Gillis J. J., Haskin L. A., Jarosewich E., Clayton R. N., Mayeda T., Fernandes V. A., Burgess R., Turner G., Eugster O., and Lorenzetti S. 2001. Northwest Africa 032: Product of lunar volcanism. *Meteoritics & Planetary Science* 37: 371–394.

Ghioroso M. S. and Sack R. O. 1995. Chemical mass transfer in magmatic processes. IV. A revised and internally consistent

thermodynamic model for the interpolation and extrapolation of liquid-solid equilibria in magmatic systems at elevated temperatures and pressures. *Contributions to Mineralogy and Petrology* 119:197–212.

Hess P. C., Rutherford M. J., and Campbell H. W. 1978. Ilmenite crystallization in non-mare basalt: Genesis of KREEP and high-Ti mare basalt. Proceedings, 9th Lunar and Planetary Science Conference. pp. 705–724.

Koeberl C., Kurat G., and Brandstatter F. 1993. Gabbroic lunar meteorites Asuka-881757 (Asuka-31) and Yamato-793169: Geochemical and mineralogical study. *Proceedings of the NIPR Symposium on Antarctic Meteorites* 6:14–34.

Neal C. R., Hacker M. D., Snyder G. A., Taylor L. A., Liu Y. G. and Schmitt R. A. 1994. Basalt generation at the Apollo 12 site, Part 1: New data, classification, and re-evaluation. *Meteoritics* 29: 334–348.

Neal C. R. and Taylor L. A. 1989. Metasomatic products of the lunar magma ocean: The role of KREEP dissemination. *Geochimica et Cosmochimica Acta* 53:529–541.

Neal C. R. and Taylor L. A. 1991. Evidence for metasomatism of the lunar highlands and the origin of whitlockite. *Geochimica et Cosmochimica Acta* 55:2965–2980.

Neal C. R. and Taylor L. A. 1992. Petrogenesis of mare-basalts: A record of lunar volcanism. *Geochimica et Cosmochimica Acta* 56:2177–2211.

Ostertag R., Amthauer G., Rager H., and McSween Jr. H. Y. 1984. Fe^{3+} in shocked olivine crystals of the ALHA 77005 meteorite. *Earth and Planetary Science Letters* 67:162–166.

Papike J. J. 1998. Comparative planetary mineralogy: Chemistry of melt-derived pyroxene, feldspar, and olivine. In *Planetary materials,* edited by Papike J. J. Washington, D.C.: Mineralogical Society of America. pp. 7.1–7.11.

Rhodes J. M., Blanchard D. P., Dungan M. A., Brannon J. C., and Rodgers K. V. 1977. Chemistry of Apollo 12 mare-basalts: Magma types and fractionation processes. Proceedings, 8th Lunar and Planetary Science Conference. pp. 1305–1338.

Rhodes J. M. and Hubbard N. J. 1973. Chemistry, classification, and petrogenesis of Apollo 15 mare-basalts. Proceedings, 4th Lunar and Planetary Science Conference. pp. 1127–1148.

Ringwood A. E. and Kesson S. E. 1976. A dynamic model for mare-basalt petrogenesis. Proceedings, 7th Lunar and Planetary Science Conference. pp. 1697–1722.

Rutherford M. J., Hess P. C., and Daniel G. H. 1974. Experimental liquid line of descent and liquid immiscibility for basalt 70017. Proceedings, 5th Lunar and Planetary Science Conference. pp. 569–583.

Ryder G. and Schuraytz B. C. 2001. Chemical variation of the large Apollo 15 olivine-normative mare-basalt rock samples. *Journal Geophysical Research* 106:1435–1451.

Shih C. Y., Nyqust L. E., Reese Y., Wiesmann H., Nazarov M. A. and Taylor L. A. 2002. The chronology and petrogenesis of the mare-basalt clast from lunar meteorite Dhofar 287: Rb-Sr and Sm-Nd isotopic studies (abstract #1344). 33rd Lunar and Planetary Science Conference. CD-ROM.

Stelzner T. H., Heide K., Bischoff A., Weber D., Schultz L., Happel M., Schron W., Neuper U., Michel R., Clayton R. N., Mayeda T. K., Bonani G., Haidas I., Ivy-Ochs S., and Suter M. 1999. An interdisciplinary study of weathering effects in ordinary chondrites from the Acfer region, Algeria. *Meteoritics & Planetary Science* 34:787–794.

Stöffler D., Keil K., and Scott E. R. D. 1991. Shock metamorphism of ordinary chondrites. *Geochimica et Cosmochimica Acta* 55: 3845–3867.

Takeda H., Arai T., and Saiki K. 1993. Mineralogical studies of lunar meteorite Yamato-793169. *Proceedings of the NIPR Symposium on Antarctic Meteorites* 6:3–13.

Taylor L. A., Kullerud G., and Bryan W. B. 1971. Opaque mineralogy and textural features of Apollo 12 samples and a comparison with Apollo 11 rocks. Proceedings, 2nd Lunar and Planetary Science Conference. pp. 855–871.

Taylor L. A., Nazarov M. A., Cohen B. A., Warren P. H., Barsukova L. D., Clayton R. N., and Mayeda T. K. 2001a. Bulk chemistry and oxygen isotopic compositions of lunar meteorites Dhofar 025 and Dhofar 026 (abstract #1985). 32nd Lunar and Planetary Science Conference. CD-ROM.

Taylor L. A., Nazarov M. A., Demidova S. I., and Patchen A. 2001b. A new lunar mare-basalt from Oman. *Meteoritics and Planetary Science* 36:A204.

Taylor L. A., Onorato P. I. K., and Uhlmann D. R. 1977. Cooling rate estimations based on kinetic modeling of Fe-Mg diffusion in olivine. Proceedings, 8th Lunar and Planetary Science Conference. pp. 1581–1592.

Taylor L. A., Patchen A., Taylor D. H. S., Chambers J. G., and McKay D. S. 1996. X-ray digital imaging petrography of lunar mare soils: Modal analysis of minerals and glasses. *Icarus* 124:500–512.

Warren P. H. and Kallemeyn G. W. 1989. Elephant Moraine 87521: The first lunar meteorite composed of predominantly mare material. *Geochimica et Cosmochimica Acta* 53:3323–3330.

Wiechert U., Halliday A. N., Lee D. C., Snyder G. A., Taylor L. A., and Rumble D. 2001. Oxygen isotopes and the moon-forming giant impact. *Science* 294:345–348.

Yanai K. and Kojima H. 1991. Varieties of lunar meteorites recovered from Antarctica. *Proceedings of the NIPR Symposium on Antarctic Meteorites* 4:70–90.